An edge-based smoothed three-node Mindlin plate element (ES-MIN3) for static and free vibration analyses of plates

***Y.B. Chai[1,2], W. Li[1,2], and Z.X. Gong[1,2]**

[1]School of Naval Architecture and Ocean Engineering, Huazhong University of Science and Technology, China
[2] Hubei Key Laboratory of Naval Architecture & Ocean Engineering Hydrodynamics (HUST), Huazhong University of Science and Technology, Wuhan City, Hubei 430074, China
*Corresponding author: cybhust@hust.edu.cn

Abstract

The smoothed finite element method (S-FEM) developed recently shows great efficiency in solving solid mechanics. This paper extends an edge-based smoothed finite element method for static and free vibration analyses of plates. The edge-based strain smoothing technique is combined with the three-node Mindlin plate element (MIN3) to give a so-called the edge-based smoothed MIN3(ES-MIN3). The system stiffness matrix is calculated by using the edge-based strain smoothing technique over the smoothing domains associated with the edges of elements. In each element the stabilized MIN3 is performed to avoid the transverse shear locking. Typical numerical examples demonstrate that the present ES-MIN3 is free of shear locking and can achieve the high accuracy compared to the exact solutions and others existing plate elements.

Keywords: Shear locking, Finite element method (FEM), Edge-based smoothed three-node Mindlin plate element (ES-MIN3), Strain smoothing technique

Introduction

Nowsdays, the plate structures have been used widely in many branches of structural engineering problems. Owing to limitations of the analytical methods, many different numerical methods, such as finite difference method, finite element method, boundary element method, meshfree method etc, have been proposed to analyze the plate structures. Among them the finite element method (FEM) is one of the most popular numerical methods to simulate the behaviors of plate structures. In the practical application, many plate elements based on the Reissner-Mindlin theory using the first-order shear deformation are preferred due to its simplicity and efficiency[Henry and Saigal (2000);Reddy (2006)]. These Reissner-Mindlin plate elements usually possess high accuracy and fast convergence speed for displacement, however, they also suffer from the ‘shear locking’ phenomenon which has the root of incorrect transverse forces under bending and induces over-stiffness as the plate become progressively thinner.

In order to eliminate shear locking and to increase the accuracy and stability of the solution, many new numerical techniques and effective modifications have been proposed, such as the mixed formulation/hybrid elements[Lee and Wong (1982); Zienkiewicz and Lefebvre (1988); Miranda and Ubertini (2006); Auricchio and Taylor(1994); Lovadina (1998)] proposed by Lee et al and Miranda et al; the enhanced assumed strain method (EAS) [Simo and Rifai (1990); Simo et al. (1989);] proposed by Simo et al and the assumed natural strain (ANS) method[Tessler and Hughes (1985); Bathe and Dvorkin (1985); Batoz and Lardeur (1989)] proposed by Hughes et al. Recently. Bletcinger et al proposed the discrete shear gap method [Bletzinger et al. (2000)] to avoid transverse shear locking and to improve the accuracy of the present formulation. In fact, the DSG also can be classified as an ANS element. It is similar to the ANS methods in the terms of modifying the course of certain strains within the element, but is different in the aspect of removing of collocation points. The DSG can work well for different elements.

Also based on the ANS method, a three-node Mindlin plate element (MIN3), which avoids shear locking, was proposed by Tessler and Hhghes. In MIN3, a complete quadratic deflection field is constrained by continuous shear edge constraints. The numerical examples demonstrated that the MIN3 is free of shear locking and can achieve convergent solutions.

Recently, Liu et al have proposed a series of smoothed finite element method (S-FEM) by incorporating the strain smoothing technique[Chen et al. (2001)] of meshfree methods into the standard finite element method. In these S-FEM models, the compatible strain fields are smoothed based on the smoothing domains created from the entities of the element mesh such as cells (CS-FEM)[Liu et al. (2001); Nguyen (2008; 2012; 2013a;2013b); Wu and Wang (2013)], or nodes (NS-FEM) [Liu et al. (2009a; 2009b); Nguyen (2011)], or edges (ES-FEM)[Liu et al. (2009c); Nguyen (2009); Li et al. (2012; 2013)],or faces (FS-FEM)[Feng et al. (2013)], then the smoothed Galerkin weak forms are evaluated based on these smoothing domains. The S-FEM models can improve significantly the accuracy of solid mechanics owing to the strain smoothing technique on the smoothing domains.

In this paper, the edge-based strain smoothing technique is incorporated with the well-known three node Mindlin plate (MIN3) to give a so-called edge-based smoothed MIN3 (ES-MIN3). In the ES-MIN3 models, the calculation of the system stiffness matrix is performed using strain smoothing technique over the smoothing domains associated with the edges of elements. The numerical results show that present method is immune from shear locking and can achieve high accurate solutions in static and vibration analysis of the Reissner-Mindlin plate.

Governing equations and weak form for the Reissner-Mindlin plate

Consider a plate under bending deformation as shown in Figure.1. The middle (neutral) surface of plate *oxy* is chosen as the reference plane that occupies a domain $\Omega \subset R^2$. Let w be the deflection of the plate and $\beta^T = (\beta_x, \beta_y)$ be the rotations of the normal to the middle surface of the plate around *y*-axis and *x*-axis, respectively. Then the unknown vector of three independent field variables at any point in the problem domain of the Reissner-Mindlin plates can be written as:

$$\mathbf{u}^T = [w \quad \beta_x \quad \beta_y] \tag{1}$$

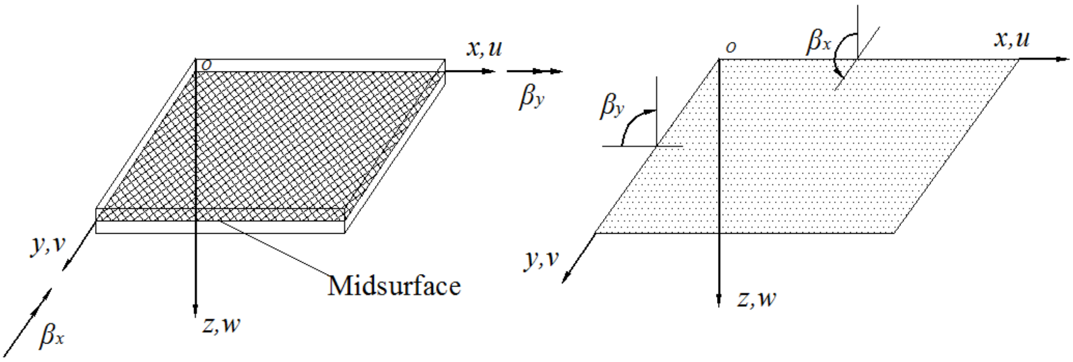

Figure.1. positive directions of displacement u, v, w and two rotation β_x, β_y for Reissner-Mindlin plate

Here we assume that the material is homogeneous and isotropic with Young's modulus E and Poisson's ratio ν. The governing differential equations of the static Reissner-Mindlin plate can be expressed as:

$$\nabla \cdot \mathbf{D}_b \boldsymbol{\kappa}(\boldsymbol{\beta}) + Gkt\boldsymbol{\gamma} = 0 \quad \text{in } \Omega \tag{2}$$

$$Gkt\nabla \cdot \boldsymbol{\gamma} + p = 0 \quad \text{in } \Omega \tag{3}$$

$$w = \bar{w}, \quad \boldsymbol{\beta} = \bar{\boldsymbol{\beta}} \quad \text{on } \Gamma = \partial\Omega \tag{4}$$

in which t is the plate thickness and $p = p(x, y)$ is a distributed load per an area unit, G and $k = 5/6$ are shear modulus and shear correction factor, respectively, $\mathbf{D}_b$ is the bending stiffness constitutive, $\boldsymbol{\kappa}$ and $\boldsymbol{\gamma}$ are the bending and shear strains, respectively, defined by

$$\kappa = \mathbf{L}_d \boldsymbol{\beta}, \quad \boldsymbol{\gamma} = \nabla w + \boldsymbol{\beta} \tag{5}$$

where $\nabla = (\partial/\partial x, \partial/\partial y)$ is the gradient vector and $\mathbf{L}_d$ denotes a matrix of differential operators:

$$L_d = \begin{bmatrix} \frac{\partial}{\partial x} & 0 & \frac{\partial}{\partial y} \\ 0 & \frac{\partial}{\partial y} & \frac{\partial}{\partial x} \end{bmatrix}^T \tag{6}$$

The standard Galerkin weakform of the static equilibrium equations for the Reissner-Mindlin plate is given by

$$\int_\Omega \delta\boldsymbol{\kappa}^T \mathbf{D}_b \boldsymbol{\kappa} d\Omega + \int_\Omega \delta\gamma^T \mathbf{D}_s \gamma d\Omega = \int_\Omega \delta w p d\Omega \tag{7}$$

where the bending stiffness constitutive coefficients $\mathbf{D}_b$ and the transverse shear stiffness constitutive coefficients $\mathbf{D}_s$ are defined as

$$\mathbf{D}_b = \frac{Et^3}{12\left(1-v^2\right)}\begin{bmatrix} 1 & v & 0 \\ v & 1 & 0 \\ 0 & 0 & 1-v/2 \end{bmatrix}, \qquad \mathbf{D}_s = ktG\begin{bmatrix} 1 & 0 \\ 0 & 1 \end{bmatrix} \tag{8}$$

For the free vibration analysis of Reissner-Mindlin plates, the standard Galerkin weak form of the dynamic equilibrium can be written as

$$\int_{\Omega} \delta\boldsymbol{\kappa}^T \mathbf{D}_b \boldsymbol{\kappa} d\Omega + \int_{\Omega} \delta\boldsymbol{\gamma}^T \mathbf{D}_s \boldsymbol{\gamma} d\Omega + \int_{\Omega} \delta\mathbf{u}^T \mathbf{m}\ddot{\mathbf{u}} d\Omega = 0 \tag{9}$$

where $\mathbf{m}$ is the mass matrix of Reissner-Mindlin plate

$$\mathbf{m} = \rho\begin{bmatrix} t & 0 & 0 \\ 0 & \dfrac{t^3}{12} & 0 \\ 0 & 0 & \dfrac{t^3}{12} \end{bmatrix} \tag{10}$$

where ρ denotes the mass density of the material.

General FEM formulation for Reissner-Mindlin plate elements

In the process of the FEM formulation of the plate, the problem domain Ω is discretized into N_e finite elements such that $\Omega_1 \cup \Omega_2 \cup \Omega_3, \cdots, \Omega_{N_e} = \Omega$ and $\Omega_i \cap \Omega_j = \varnothing$, $i \neq j$,where N_e is the number of total elements. Then the finite element solution $\mathbf{u} = \begin{bmatrix} w & \beta_x & \beta_y \end{bmatrix}$ of a displacement model for the Reissner-Mindlin plate can be expressed as

$$\mathbf{u} = \sum_{I=1}^{N_n} \begin{bmatrix} N_I(\mathbf{x}) & 0 & 0 \\ 0 & N_I(\mathbf{x}) & 0 \\ 0 & 0 & N_I(\mathbf{x}) \end{bmatrix} \mathbf{d}_I \tag{11}$$

where N_n is the number of total nodes of problem domain, $N_I(\mathbf{x})$ is the shape function at node I , $\mathbf{d}_I = \begin{bmatrix} w_I & \beta_{xI} & \beta_{yI} \end{bmatrix}^T$ is the nodal displacement vector associated to node I.
Then the bending and shear strains can be expressed as

$$\begin{aligned} \boldsymbol{\kappa} &= \sum_I \mathbf{B}_{bI} \mathbf{d}_I \\ \boldsymbol{\gamma} &= \sum_I \mathbf{B}_{sI} \mathbf{d}_I \end{aligned} \tag{11}$$

where

$$\mathbf{B}_{bI} = \begin{bmatrix} 0 & \partial N_I/\partial x & 0 \\ 0 & 0 & \partial N_I/\partial y \\ 0 & \partial N_I/\partial y & \partial N_I/\partial x \end{bmatrix} \tag{12}$$

$$\mathbf{B}_{sI} = \begin{bmatrix} \partial N_I/\partial x & N_I & 0 \\ \partial N_I/\partial y & 0 & N_I \end{bmatrix} \tag{13}$$

The discretized system stiffness matrix, $\mathbf{K}$ can be expressed in terms of its bending, $\mathbf{K}_b$,and transverse shear, $\mathbf{K}_s$,components as

$$\begin{aligned} \mathbf{K} = \mathbf{K}_b + \mathbf{K}_s &= \int_{\Omega} \mathbf{B}_b^T \mathbf{D}_b \mathbf{B}_b d\Omega + \int_{\Omega} \mathbf{B}_s^T \mathbf{D}_s \mathbf{B}_s d\Omega \\ &= \sum_{i=1}^{N_e} \int_{\Omega_i^e} \mathbf{B}_b^T \mathbf{D}_b \mathbf{B}_b d\Omega + \sum_{i=1}^{N_e} \int_{\Omega_i^e} \mathbf{B}_b^T \mathbf{D}_b \mathbf{B}_b d\Omega \end{aligned} \tag{14}$$

For static analysis, the discretized system equations of the Reissner-Mindlin plate can be expressed as

$$\mathbf{Kd} = \mathbf{F} \tag{15}$$

where $\mathbf{F}$ is the load vector and has the form of

$$\mathbf{F} = \int_{\Omega} \mathbf{N}^T p d\Omega + f_b = \sum_{i=1}^{N_e} \int_{\Omega_i^e} \mathbf{N}^T p d\Omega + f_b \tag{16}$$

in which f_b relates to the prescribed boundary loads.
For the free vibration, the force form vanishes and we shall have

$$\left(\mathbf{K} - \omega^2 \mathbf{M}\right)\mathbf{d} = \mathbf{0} \tag{17}$$

where ω is the natural frequency of the free vibration and $\mathbf{M}$ is the global mass matrix

$$\mathbf{M} = \int_{\Omega} \mathbf{N}^T \mathbf{m} \mathbf{N} d\Omega = \sum_{i=1}^{N_e} \int_{\Omega_i^e} \mathbf{N}^T \mathbf{m} \mathbf{N} d\Omega \tag{18}$$

Formulation of the MIN3

The main assumption of MIN3 is that the rotations are linear through the rotational DOFs at three nodes of the elements and deflection is quadratic through the deflection DOFs at six nodes (three nodes of the elements and three mid-edge points). The deflection DOFs at three mid-edge points can be removed by enforcing continuous shear constraints at every element edge, and then the deflection is approximated only by vertex DOFs at three nodes of the elements. Numerical examples demonstrated that the MIN3 element can overcome shear-locking-free and produces convergent solutions [Tessler and Hughes (1985)].

As shown in Figure.2, using the three-node triangular element mesh, the linear rotations β_x and β_y can be expressed as

$$\begin{aligned} \beta_x &= \sum_{I=1}^{3} N_I(\mathbf{x})\beta_{xI} = \mathbf{N}\boldsymbol{\beta}_x \\ \beta_y &= \sum_{I=1}^{3} N_I(\mathbf{x})\beta_{yI} = \mathbf{N}\boldsymbol{\beta}_y \end{aligned} \tag{19}$$

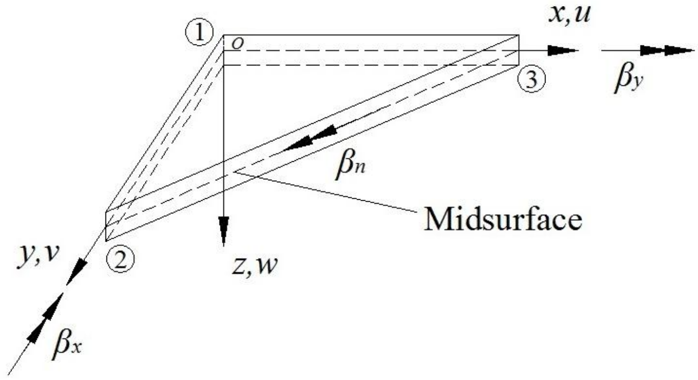

Figure. 2 Three-node triangular element

And the initial quadratic deflection w can be expressed as

$$w = \sum_{I=1}^{6} R_I w_I = \mathbf{R} w_{ini} \tag{20}$$

where $\mathbf{N} = \left[N_1(x) \quad N_2(x) \quad N_3(x) \right]$ are the linear shape functions at node I . $\boldsymbol{\beta}_x^T = \left[\beta_{x1} \quad \beta_{x2} \quad \beta_{x3} \right]$ and $\boldsymbol{\beta}_y^T = \left[\beta_{y1} \quad \beta_{y2} \quad \beta_{y3} \right]$ are the rotational DOFs at three nodes of the element; $\mathbf{w}_{ini}^T = \left[w_1 \quad w_2 \quad w_3 \quad w_4 \quad w_5 \quad w_6 \right]$ is the deflection DOFs at six nodes (three nodes of the elements and three mid-edge points as shown in Table. 1), and R is the row vector of quadratic shape functions given by

$$R_i = N_i(2N_i - 1), \; R_{i+3} = 4N_i N_k \;\; (i = 1,2,3; k = 2,3,1) \tag{21}$$

Table 1 Nodal configuration for initial (unconstrained) and constrained displacement

Shape functions		Initial nodal configuration	Continuous shear edge constraints $(w_{,s} + \beta_n)_{,s}\big|_{\text{edges}} = 0$	Constrained nodal configuration
w	β_x, β_y			
Quadratic	Linear	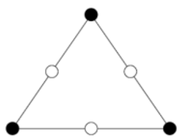	Three edge constraints	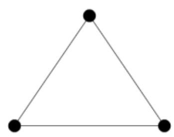

Equations (19) and (20) can be directly used in formulating element matrices. However, it may be advantageous from the standpoint of nodal simplicity to condense out the mid-edge deflection

DOFs, w_4, w_5 and w_6 in w. This can be accomplished by enforcing continuous shear constraints at every element edge as given by the following differential relation

$$(w_{,s} + \beta_n)_{,s}\Big|_{\text{edges}} = 0 \tag{22}$$

where s denotes the edge coordinate and β_n is the tangential edge rotation as shown in Figure.2. The enforcement of constraint (21) at three element edges yields

$$\begin{gathered} w_{i+3} = \frac{1}{2}(w_i + w_j) + \frac{1}{8}\left[b_k(\beta_{xi} - \beta_{xj}) + a_k(\beta_{yj} - \beta_{yi})\right] \\ \left(i = 1,2,3;\ j = 2,3,1; k = 3,1,2\right) \end{gathered} \tag{23}$$

where $a_1 = x_3 - x_2$, $a_2 = x_1 - x_3$, $a_3 = x_2 - x_1$, $b_1 = y_2 - y_3$, $b_2 = y_3 - y_1$, $b_3 = y_1 - y_2$ as shown in Figure.3.

By substituting (23) into (20), there results a constrained deflection field exclusively in terms of vertex DOFs.

$$w = \sum_{I=1}^{3} N_I w_I + \sum_{I=1}^{3} H_I \beta_{xI} + \sum_{I=1}^{3} L_I \beta_{yI} = \mathbf{Nw} + \mathbf{L\beta}_x + \mathbf{H\beta}_y \tag{24}$$

where $\mathbf{w}^T = \begin{bmatrix} w_1 & w_2 & w_3 \end{bmatrix}$, $\mathbf{H} = \begin{bmatrix} H_1 & H_2 & H_3 \end{bmatrix}$, $\mathbf{L} = \begin{bmatrix} L_1 & L_2 & L_3 \end{bmatrix}$ are the vectors of shape functions, with, $I = 1,2,3$, given by

$$\begin{aligned} H_1 &= \frac{1}{2}(a_2 N_3 N_1 - a_3 N_1 N_2) \\ H_2 &= \frac{1}{2}(a_3 N_1 N_2 - a_1 N_2 N_3) \\ H_3 &= \frac{1}{2}(a_1 N_2 N_3 - a_2 N_3 N_1) \\ L_1 &= \frac{1}{2}(b_3 N_1 N_2 - b_2 N_3 N_1) \\ L_2 &= \frac{1}{2}(b_1 N_2 N_3 - b_3 N_1 N_2) \\ L_3 &= \frac{1}{2}(b_2 N_3 N_1 - b_1 N_2 N_3) \end{aligned} \tag{25}$$

Then the element stiffness matrix can be finally obtained and written in the following form:

$$\mathbf{K}_e^{\text{MIN3}} = \int_{\Omega_e} \mathbf{B}_b^T \mathbf{D}_b \mathbf{B}_b d\Omega + \int_{\Omega_e} \mathbf{B}_s^T \mathbf{D}_s \mathbf{B}_s d\Omega \tag{26}$$

where

$$\mathbf{B}_b = \begin{bmatrix} 0 & \partial N_I/\partial x & 0 \\ 0 & 0 & \partial N_I/\partial y \\ 0 & \partial N_I/\partial y & \partial N_I/\partial x \end{bmatrix} \tag{27}$$

$$\mathbf{B}_s = \begin{bmatrix} \partial N_I/\partial x & \partial L_I/\partial x & \partial H_I/\partial x + N_I \\ \partial N_I/\partial y & \partial L_I/\partial x + N_I & \partial H_I/\partial y \end{bmatrix} \tag{28}$$

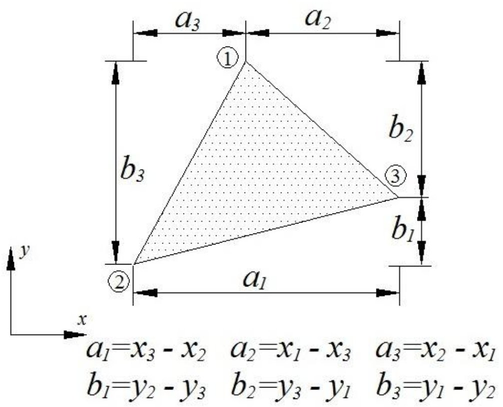

Figure.3 Three-node triangular element coordinate description

In order to further improve the accuracy of approximate solutions and to stabilize shear force oscillations. It was suggested that $\mathbf{D}_s$ in (8) should be replaced by $\hat{\mathbf{D}}_s$

$$\hat{\mathbf{D}}_s = \frac{Gkt}{t^2 + \alpha h_e^2} \tag{29}$$

In which h_e is the longest length of the edges of the element and α is a positive constant [Lyly and Stenberg (1993)].

Formulation of ES-MIN3

In this section, a new triangular element named an edge-based smoothed triangular element is established by combining the edge-based strain smoothing technique with the MIN3 (ES-MIN3). In this work, we incorporate the ES-FEM with the MIN3 to give a so-called ES-MIN3 for the plate elements. In the ES-MIN3, we do not use the compatible strain fields as in (11) but the smoothed strain fields over local smoothing domains associated with the edges of elements. Naturally the numerical integrations in (14) for the stiffness matrix are no longer based on elements as in standard FEM but on the edge-based smoothing domain Ω_k ($k = 1, 2, \cdots, N$), where N is the total number of edges in the 2D problem domains, for triangular elements, the smoothing domain for edge k is created by sequentially connecting two end points of the edge and centroids of its surrounding elements. As shown in Figure.4, for interior edges, the smoothing domain Ω_k for edge k is formed by assembling two sub-domains of two neighboring elements; while for global boundary edge, the smoothing domain Ω_k of edge k is a single sub-domain, in this case, the strain and stain matrix can be calculated as same as those in FEM.

In the present method, smoothing operation is applied over each smoothing domain, so the smoothed bending strain $\bar{\kappa}$ and smoothed shear stain $\bar{\gamma}$ can be calculated by

$$\bar{\kappa}_e = \int_{\Omega_e} \kappa W\left(x\right) d\Omega$$
$$\bar{\gamma}_e = \int_{\Omega_e} \gamma W\left(x\right) d\Omega \tag{30}$$

where $W\left(x\right)$ is a given smoothing function that satisfies at least unity property

$$\int_{\Omega_k} W_k(\mathbf{x}) d\Omega = 1 \tag{31}$$

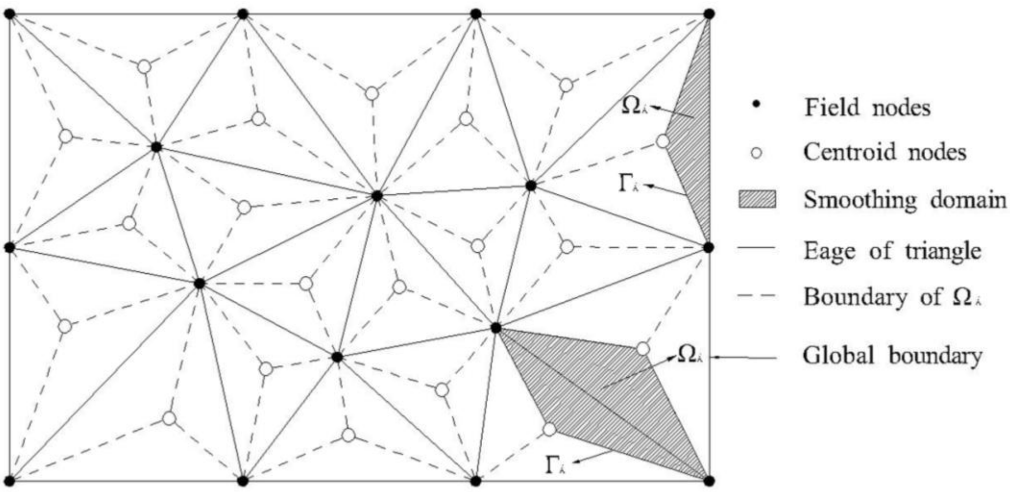

Figure. 4. Edge-based smoothing domains in 2D problem created by sequentially connecting the centroids of the adjacent triangles with the end-points of the edge.

In this study, the following simplest form of the smoothing function is used

$$W_k(\mathbf{x}) = \begin{cases} 1/A_k & x \in \Omega_k \\ 0 & x \notin \Omega_k \end{cases} \tag{32}$$

where A_k is the area of the smoothing domain of the *k*th edge and is computed by

$$A_k = \int_{\Omega_k} d\Omega = \frac{1}{3}\sum_{j=1}^{n_k^e} A_j^e \tag{33}$$

where n_k^e is the number of elements around the edge k ($n_k^e = 1$ for the boundary edges and $n_k^e = 2$ for inner edges, as shown in Figure. 4), A_j^e is the area of the j th element around the edge k .

By using the edge-based strain smoothing operation, the smoothed strain of the smoothed strain of the smoothing domain Ω_k^s in (30) can be expressed as follows

$$\bar{\kappa}_k = \frac{1}{A_k^s}\int_{\Omega_k^s} \kappa d\Omega = \frac{1}{A_k^s}\sum_{q=1}^{n_s} A_{k,q} \cdot \kappa_{k,q}$$
$$\bar{\gamma}_k = \frac{1}{A_k^s}\int_{\Omega_k^s} \gamma d\Omega = \frac{1}{A_k^s}\sum_{q=1}^{n_s} A_{k,q} \cdot \gamma_{k,q} \tag{34}$$

where $A_{k,q}$ denotes the area of the sub-smoothing domain associated with inner edge k, $\kappa_{k,q}$ and $\gamma_{k,q}$ are bending strain and shear strain of the qth sub-smoothing domain, respectively. With the above formulation, the smoothed strains for the smoothing domain of edge k can be expressed in the following forms:

$$\begin{aligned}\bar{\kappa}_k &= \sum_{I=1}^{M_k} \bar{\mathbf{B}}_{b,I}\left(x_k\right)\cdot d_I \\ \bar{\gamma}_k &= \sum_{I=1}^{M_k} \bar{\mathbf{B}}_{s,I}\left(x_k\right)\cdot d_I\end{aligned} \tag{35}$$

where M_k is the total number of nodes in the influence domain of edge k, $\bar{B}_{b,I}\left(x_k\right)$ and $\bar{B}_{s,I}\left(x_k\right)$ are termed as the smoothed strain matrix that can be calculated as

$$\begin{aligned}\bar{\mathbf{B}}_{b,I}\left(x_k\right) &= \frac{1}{A_k}\sum_{i=1}^{M_k}\frac{1}{3}A_i\mathbf{B}_{bi}\left(x_k\right) \\ \bar{\mathbf{B}}_{s,I}\left(x_k\right) &= \frac{1}{A_k}\sum_{i=1}^{M_k}\frac{1}{3}A_i\mathbf{B}_{si}\left(x_k\right)\end{aligned} \tag{36}$$

Therefore the global stiffness matrices of the ES-MIN3 element can be assembled by

$$\bar{\mathbf{K}}_k = \sum_{i=1}^{n_k}\mathbf{K}_k \tag{37}$$

where K_k is the smoothed element stiffness matrix given by

$$\bar{\mathbf{K}}_k = \int_{\Omega_k}\bar{\mathbf{B}}_b^T\mathbf{D}_b\bar{\mathbf{B}}_b d\Omega + \int_{\Omega_k}\bar{\mathbf{B}}_s^T\mathbf{D}_s\bar{\mathbf{B}}_s d\Omega = \bar{\mathbf{B}}_b^T\mathbf{D}_b\bar{\mathbf{B}}_b A_k + \bar{\mathbf{B}}_s^T\mathbf{D}_s\bar{\mathbf{B}}_s A_k \tag{38}$$

The procedure of assembling the global stiffness matrix in the ES-MIN3 is exactly the same as the practice in the standard FEM. It can be easily seen from (37) that the resultant linear system is symmetric and banded (due to the compact supports of FEM shape functions), which implies that the system equation can be solved efficiently.

Numerical results

Static analysis

Consider a flexible rectangular plate (0.314m × 0.414m) which is made of aluminum (ρ =2700kg/m^3, ν =0.3, and E =71GPa). The thickness of the plate is 0.001m. The plate is subjected to a uniform load of $q(x, y)$ =1Pa, and is given for clamp boundary condition. Uniform meshes of $2\times N\times N$ three-node triangular plate elements shown in Figure.5 is used in the computation, where N denotes the number of elements per edge.

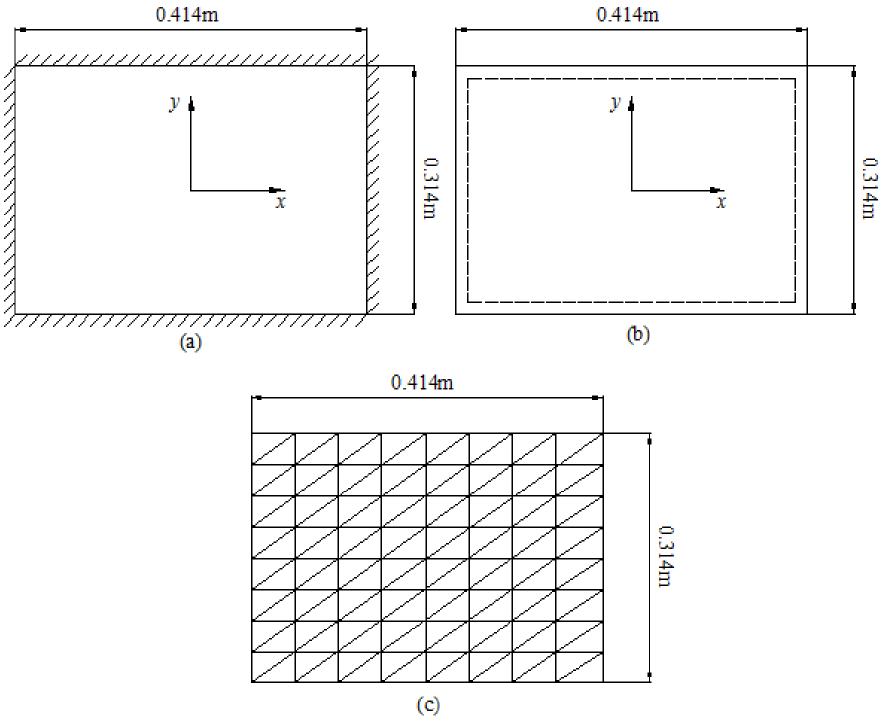

Figure 5 Two rectangular plate models and the representative meshes: (a) clamped plate; (b) simply supported plate; (c) regular mesh using three-node triangular elements

For static analysis, the deflection at the center point of the plate is computed; the result is plotted against the mesh density in terms of number of elements per edge *N*, as shown in Figure.6. It is seen that the ES-MIN3 achieves the higher accuracy compared to the DSG and MIN3 elements.

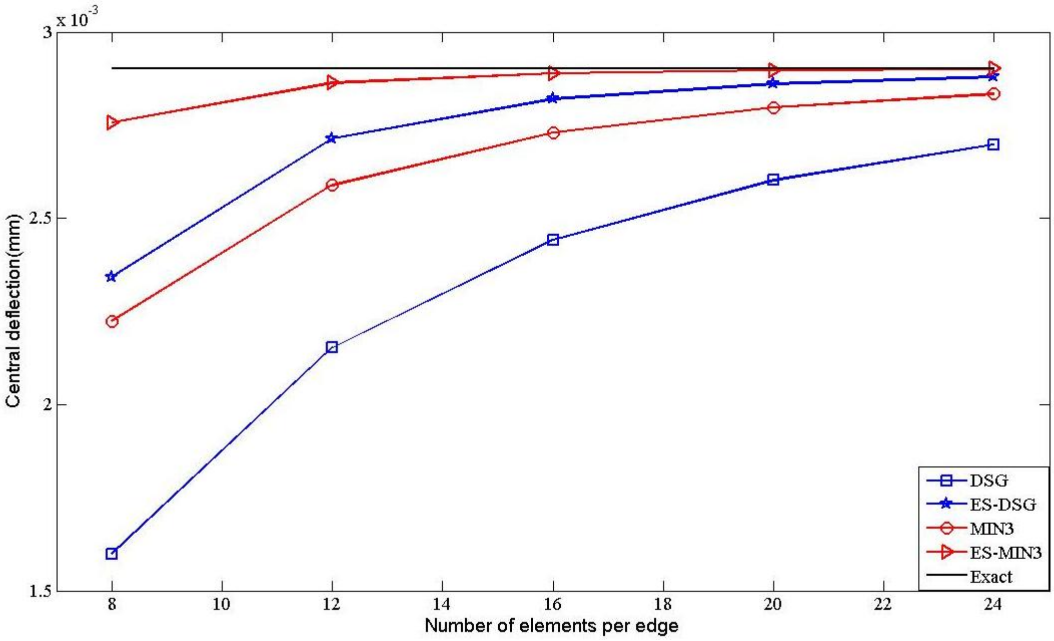

Figure 6 Convergence of deflection of the plate at the center against the mesh density

Free vibration analysis of plates

In this section, we investigate the performance of the ES-MIN3 used for computing the natural frequencies of plates. The geometry and material parameters of the plate are the same as in last section. All the edges of the plate are simply-supported and five uniform meshes of $2\times N\times N$ three-node triangular plate elements with N=8, 12, 16, 20, 24 are used in the computation. The first six natural frequencies of the plate obtained from ES-MIN3 are listed in Table 2, for comparison, the analytical solutions and some other numerical results are also listed in the table. As indicated in the table, all the numerical results are in good agreement with the analytical results in low frequency range. The errors of the results for all these numerical methods become larger with the increasing of mode order. However, the results obtained using ES-MIN3 is much more accurate and converged much faster than those obtained using other methods. It is confirmed that the ES-MIN3 is efficient and can give high accurate solutions in free vibration analysis. In particular, the ES-MIN3 can achieve accurately the values of high frequencies of plate by using only coarse meshes.

Table 2 Convergence of the first six natural frequencies (Hz) of the plate

Meshing	Methods	Mode sequence number					
		1	2	3	4	5	6
8	DSG	43.87	99.74	138.23	190.09	243.67	313.86
	ES-DSG	39.93	88.57	122.37	172.39	191.12	277.93
	MIN3	41.95	96.03	130.66	186.66	220.30	301.90
	ES-MIN3	39.86	87.09	120.98	171.40	178.50	271.09
12	DSG	41.71	92.82	125.83	173.07	204.74	272.24
	ES-DSG	39.32	84.41	116.79	161.88	168.01	251.05
	MIN3	40.27	88.14	120.48	168.61	182.61	263.15
	ES-MIN3	39.33	83.88	116.36	161.27	163.64	244.26
16	DSG	40.63	88.97	120.61	165.99	186.77	257.54
	ES-DSG	39.13	83.05	115.06	158.00	161.48	239.85
	MIN3	39.67	85.25	117.14	162.07	169.95	251.07
	ES-MIN3	39.15	82.84	114.88	157.55	159.77	236.19
20	DSG	40.04	86.62	117.94	162.08	176.45	250.25
	ES-DSG	39.05	82.47	114.31	156.07	159.02	234.67
	MIN3	39.40	83.89	115.63	158.91	164.29	243.79
	ES-MIN3	39.07	82.38	114.21	155.77	158.21	232.69
24	DSG	39.69	85.15	116.42	159.65	170.07	246.09
	ES-DSG	39.00	82.17	113.91	155.00	157.85	232.00
	MIN3	39.25	83.15	114.82	157.10	161.34	238.58
	ES-MIN3	39.02	82.13	113.86	154.81	157.42	230.83
	Analytical	38.95	81.61	113.11	152.72	155.78	226.89

Conclusions

In this work, the edge-based smoothed finite element method is combined with the well-known MIN3 to give a so-called the ES-MIN3 for static and free vibration analyses of plates. The smoothed Galerkin weak form is adopted to formulate the discretized system equations. The numerical integration is performed over the smoothing domains associated with edges of mesh. Through the formulation and the numerical examples, some concluding remarks can be drawn as follows:

1) The ES-MIN3 is straightforward and the implementation is as easy as MIN3 for the static and free vibration analyses of plates.
2) The shear locking of the triangular plate elements has been successfully alleviated with ES-MIN3 and the ES-MIN3 elements have only three DOFs at each vertex node without additional degrees of freedom, in addition, the ES-MIN3 only use the triangular elements which is a clear adbantage compared to quadrilateral elements when the geometry domain of plate is complicated.
3) For both static and free vibration analyses, the results of the ES-MIN3 agree well with other methods. The ES-MIN3 gives much more accurate results than the DSG, MIN3 and is a good competitor to the ES-DSG.
4) The ES-MIN3 works very well with triangular meshes and it is thus very promising to solve real engineering problems which usually are of complicated geometries with very accurate results.

References

Henry, T. Y., Saigal. S., Masud, A., Kapania, R. K. (2000) A survey of recent shell finite elements, *International Journal for Numerical Methods in Engineering* **47**, 101–127.

Reddy, J. N, (2006) Theory and analysis of elastic plates and shells.CRC Press, Taylor and Francis Group, New York

Lee, S. W., Wong, C. (1982) Mixed formulation finite elements for Mindlin theory platebending, *International Journal for Numerical Methods in Engineering* **18**, 1297–1311.

Zienkiewicz, O. C., Lefebvre, D. (1988) A robust triangular plate bending element of the Reissner–Mindlin type, *International Journal for Numerical Methods in Engineering* **26**, 1169–1184.

Miranda, S. D., Ubertini, F.(2006) A simple hybrid stress element for shear deformable plates, *International Journal for Numerical Methods in Engineering* **65**, 808–833.

Auricchio, F., Taylor, R. L. (1994) A shear deformable plate element with an exact thin limit, *Computer Methods in Applied Mechanics and Engineering* **65**, 393–412.

Lovadina, C. (1998) Analysis of a mixed finite element method for the Reissner–Mindlin plate problems, *Computer Methods in Applied Mechanics and Engineering* **163**, 71–85.

Simo, J. C., Rifai, M. S. (1990) A class of mixed assumed strain methods and the method of incompatible modes, *International Journal for Numerical Methods in Engineering* **29**, 1595–1638.

Simo, J. C., Fox, D.D., Rifai, M. S. (1989) On a stress resultant geometrically exact shell model. Part II: The linear theory, computational aspects, *Computer Methods in Applied Mechanics and Engineering* **73**, 53–92.

Tessler, A., Hughes, T. J. R. (1985) A three-node Mindlin plate element with improved transverse shear, *Computer Methods in Applied Mechanics and Engineering* **50**, 71–101.

Bathe, K. J., Dvorkin, E. N. (1985) A four-node plate bending element based on Mindlin/Reissener plate theory and a mixed interpolation, *International Journal for Numerical Methods in Engineering* **21**, 367–383.

Batoz, J. L., Lardeur, P. (1989) A discrete shear triangular nine d.o.f. element for the analysis of thick to very thin plates, *International Journal for Numerical Methods in Engineering* **29**, 533–560.

Bletzinger, K. U., Bischoff, M., Ramm, E. (2000) A unified approach for shear-locking free triangular and rectangular shell finite elements, *Computers and Structures* **75**, 321–334.

Chen, J. S., Wu, C. T., Yoon, S. You, Y. (2001) A stabilized conforming nodal integration forGalerkin mesh-free methods, *International Journal for Numerical Methods in Engineering* **50**, 435–466.

Liu, G. R., Dai, K. Y. and Nguyen, T. T. (2007) A smoothed finite element method for mechanics problems, *Computational Mechanics* **39**, 859–877.

Nguyen, T. T., Rabczuk, T., Nguyen, X. H., Bordas, S. (2008) A smoothed finite element method for shell analysis, *Computer Methods in Applied Mechanics and Engineering* **198**, 165–177.

Nguyen, T. T., Phung, V. P., Thai, C. H., Nguyen, X. H. (2012) A cell-based smoothed discrete shear gap method using triangular elements for static and free vibration analyses of Reissner–Mindlin plates, *International Journal for Numerical Methods in Engineering* **91**, 705–741.

Nguyen, T. T., Phung, V. P., Thai, C. H., Nguyen, X. H. (2013a) A cell-based smoothed discrete shear gap method (CS-DSG3) using triangular elements for static and free vibration analyses of shell structures, *International Journal of Mechanical Sciences* **74**, 32–45.

Nguyen, T. T., Phung, V. P., H. Luong, V. H., Nguyen, V. H., Nguyen, X. H. (2013b) A cell-based smoothed three-node Mindlin plate element (CS-MIN3) for static and free vibration analyses of plates, *Computational Mechanics*, **51**, 65–81.

Wu, C. T., Wang, H. P. (2013) An enhanced cell-based smoothed finite element method for the analysis of Reissner–Mindlin plate bending problems involving distorted mesh, *International Journal for Numerical Methods in Engineering* **95**, 288–312.

Liu, G. R., Nguyen, T. T., and Zeng, K. (2009a). A novel singular node based smoothed finite element method (NS-FEM) for upper bound solutions of fracture problems, *International Journal for Numerical Methods in Engineering*, **83**, 1466–1497.

Liu, G. R., Nguyen, T. T., Nguyen, X. H. and Lam, K. Y. (2009b) A node-based smoothed finite element method (NS-FEM) for upper bound solutions to solid mechanics problems, *Computers and Structures* **87**, 14–26.

Nguyen, T. T., Liu, G. R., Nguyen, X. H. and Nguyen, X. C. (2011) Adaptive analysis using the node-based smoothed finite element method (NS-FEM) , *International Journal for Numerical Methods in Engineering*, **27**, 198–218.

Liu, G. R., Nguyen, T. T., and Lam, K. Y. (2009c) An edge-based smoothed finite element method (ES-FEM) for static, free and forced vibration analysis of solids, *Journal of Sound and Vibration*, **320**, 1100–1130.

Nguyen, X. H., Liu, G. R., Thai, H. C., and Nguyen, T. T. (2009) An edge based smoothed finite element method with stabilized discrete shear gap technique for analysis of Reissner–Mindlin plates, *Computer Methods in Applied Mechanics and Engineering* **199**, 471–489.

Li, W., Chai, Y. B., Lei, M. and Liu, G. R. (2013) Analysis of Coupled Structural-Acoustic Problems Based on the Smoothed Finite Element Method (S-FEM), 4th International Conference on Computational Methods, Golded Coast, Australia.

Li, W., Lei, M., Chai, Y. B. and Liu, G. R. (2013) Analysis of Exterior Acoustics using the Edge-based Smoothed Finite Element Method (ES-FEM), APCOM & ISCM 2013，Singapore.

Feng, S. Z., Cui, X. Y., Liu, G. R. (2013) Transient thermal mechanical analyses using a face-based smoothed finite element method (FS-FEM), *International Journal of Thermal Sciences*, **74**, 95–103.
Lyly, M., Stenberg, R.,Vihinen, T. (1993) A stable bilinear element for the Reissner–Mindlin plate model, *Computer Methods in Applied Mechanics and Engineering* **110**, 343–357.